Conductivity and Electrical Properties of Chitosan - Methylcellulose Blend Biopolymer Electrolyte Incorporated with Lithium Tetrafluoroborate

Yahya A.K. Salman [1], Omed Gh. Abdullah [2,3,], Rawad R. Hanna [1], Shujahadeen B. Aziz [2,3]*

[1] Department of Physics, College of Science, University of Mosul, 41002, Mosul, Iraq.
[2] Advanced Polymeric Materials Research Lab., Department of Physics, College of Science, University of Sulaimani, 46001, Kurdistan Region, Iraq.
[3] Komar Research Center, Komar University of Science and Technology, 46001, Sulaimani, Kurdistan Region, Iraq.
[*]E-mail: omed.abdullah@univsul.edu.iq

This work focuses on the structural and electrical properties of solid biopolymer blend electrolytes based on chitosan and methylcellulose incorporated with lithium tetrafluoroborate ($LiBF_4$). The polymer electrolyte films were prepared by solution casting technique. The polymer blend comprised of 75 wt.% chitosan and 25 wt.% methylcellulose, the most amorphous blend composition are used as the host matrix. Fourier transform infrared (FT-IR) spectroscopy analysis demonstrated the interactions between biopolymer blend and $LiBF_4$. The highest value of electrical conductivity at ambient temperature 3.74×10^{-6} S cm^{-1} was obtained for the sample containing 40 wt.% $LiBF_4$. All electrolyte samples were found to obey the Arrhenius rule. The magnitude of activation energy decreases with increasing electrical conductivity and vice-versa. Rice and Roth model was applied to analyze the electrical conductivity enhancement. The temperature dependence of the frequency exponent (*s*) shows that the conduction mechanism depends on the salt concentration, the appropriate model for low concentration was found to be correlated barrier hopping (CBH) model, while for high salt concentration samples follow the non-overlapping small polaron tunneling (NSPT) model.

1. INTRODUCTION

Different solid polymer electrolyte systems have been intensively studied owing to their potential application in electrical energy-storage devices that require flexible thin-film with high performance, such as solar cells, solid-state rechargeable batteries, fuel cells and electrochemical double-layer capacitors [1,2]. In contrast to conventional organic liquid electrolytes, solid polymer

electrolytes possess particular essential properties such as ease and low-cost fabrication, excellent electrochemical stability, safety, cyclability, good shelf life and processability [3].

Natural biopolymers such as chitosan and methylcellulose have attracted significant consideration in recent works due to their advantages, such as water-soluble, biodegradable, biocompatible, non-toxic, abundance and excellent film-forming properties [4,5].

Much effort has been harnessed to produce solid polymer electrolyte films based on chitosan, methylcellulose and their blend [6,7]. Chitosan is a linear polysaccharide composed of randomly distributed β-(1→4)-linked D-glucosamine and N-acetyl-D-glucosamine units which can be prepared by deacetylation of chitin [8,9]. Chitosan has a large number of functional groups including hydroxyl group, acetamido group, and amino group that can act as electron donors [10]. Methylcellulose is a polysaccharide that consists of β-(1→4) glucosidic units with methyl substituent in linear chains. It can be prepared from the reaction of alkali-cellulose with dimethyl sulfate or methyl chloride [11].

The combination of salt and polymers is an important technique to provide ions as the charge carriers. Different lithium salts such as lithium perchlorate ($LiClO_4$) [12], lithium hexafluorophosphate ($LiPF_6$) [13], and lithium triflate ($LiCF_3SO_3$) [14] are commonly used to prepare solid polymer electrolytes due to the fact that lithium-ion is the lightest of all metals, has the greatest electrochemical potential, and could provide the largest energy content [15]. Ulaganathan and Rajendran [16] used different lithium salts ($LiBF_4$, $LiClO_4$, and $LiCF_3SO_3$) to prepare polymer electrolyte based on poly(vinyl acetate) (PVAc), and poly(vinylidene fluorideco-hexafluoropropylene) (PVdF-co-HFP) as a host matrix. They reported that the $LiBF_4$ salt exhibits higher conductivity due to the lowest lattice energy compared to other lithium salts. Sudhakar and Selvakumar [12] reported the high room-temperature electrical conductivity of 1.20×10^{-7} S cm^{-1} for a starch-chitosan blend biopolymer electrolyte films incorporated with lithium perchlorate ($LiClO_4$). A plasticized biopolymer electrolyte based on a methylcellulose-chitosan blend incorporated with NH_4NO_3-EC gives the highest electrical conductivity of 2.16×10^{-4} S cm^{-1} at ambient temperature, as reported by Zazuli and Khiar [17].

To the best of the author's knowledge, there are no systematic studies on lithium solid biopolymer electrolytes based on a chitosan-methylcellulose blend. In our previous work [18] it has been shown that the blend comprising 75 wt.% chitosan and 25 wt.% methylcellulose served as a perfect host matrix for conduction due to its more amorphous nature compared to other compositions. This work aimed to develop lithium ion conducting biopolymer electrolyte films based on chitosan-methylcellulose blend incorporated with different amounts of lithium tetrafluoroborate ($LiBF_4$). The samples will then be characterized by X-ray diffraction (XRD), Fourier transform infrared (FTIR) spectroscopy, Scanning electron microscopy (SEM), and impedance spectroscopy (EIS) to study the impact of salt concentration on the ionic conductivity, as well as the conduction mechanism.

2. EXPERIMENTAL METHODS

2.1 Preparation of pure chitosan-methylcellulose blend film

The pure polymer blend sample based on chitosan-methylcellulose in the ratio of 75:25 was prepared by dissolving 1.5 gm of chitosan powder in 150 ml of 2% acetic acid, and 0.5 gm of methylcellulose in 20 ml distilled water separately, at ambient temperature. The two solutions were

stirred continuously using a magnetic stirrer for two days, until the powders are completely dissolved, to obtain clear viscose solutions. Then, these two solutions were mixed under continuous stirring until homogeneous viscous solution was obtained, the obtained solution was cast onto plastic Petri dish and allowed to dry at room temperature. The film was kept in a desiccator with silica-gel desiccant for the further drying process.

2.2. Preparation of solid polymer electrolyte films

Polymer blend electrolyte films were prepared by adding different amounts of $LiBF_4$ (5, to 50 wt.% with step of 5 wt.%) into the solution of chitosan-methylcellulose in the ratio 75:25. The solution was stirred until it became homogeneous. The obtained homogeneous solutions were cast onto different plastic Petri dishes and left for drying process at room temperature to form a film. The dried films were peeled and kept in a desiccator filled with silica gel desiccants for further drying. The average thicknesses of the prepared films were between 135 and 237 μm.

2.3. Solid polymer electrolytes characterization

X-ray diffraction (XRD) measurements of the solid polymer blend electrolytes were performed using X-ray diffractometer (X'PERT-PRO) where Cu Kα source generated X-rays with wavelengths, λ=1.5406 Å. The glancing angle (2θ) was varied from 10° to 70° with a step size of 0.1°.

The FTIR studies were carried out using Frontier Perkin-Elmer spectrometer in the wavenumber range of 4000-400 cm^{-1} with the minimum resolution of 1 cm^{-1}. The objective of FTIR was to confirm complex formation between the blend polymer and the lithium salt.

The surface morphology of the solid polymer electrolyte films was examined by scanning electron microscope (Tescan Vega 3) at 5000× magnification. The polymer sample was sputtered with gold using a sputter-coater unite (Emitech K550X) for 3 min at 25 mA.

The electrical conductivity of the samples was measured using the Precision LCR Meter (Agilent/HP 4284 A) at a frequency range of 100 Hz - 1 MHz, and over the temperature range from 295K to 363 K. The polymer electrolyte films were sandwiched between two aluminium electrodes with a diameter of 250 mm, and the measurements were carried out in the conduction mode. The sample temperature has been monitored using a T-type thermocouple with an accuracy of ±1 °C. The ac conductivity (σ_{ac}) was calculated from the measured value of conductivity (G) using: $\sigma_{ac}(\omega) = Gd/A$, where d is the thickness of the prepared film, and A is the electrode-specimen contact cross-sectional area.

3. RESULTS AND DISCUSSION

3.1. XRD analysis

From the X-ray diffraction pattern of the chitosan-methylcellulose blend film in figure 1-a, a semicrystalline diffraction peak appears at 2θ = 21.1°, which is comparable with the chitosan peak (2θ = 20.0°) obtained by Hasegawa et al. [19]. This semicrystalline peak results from the strong

intermolecular interaction between polymer chains through the intermolecular hydrogen bonding [20]. Earlier studies on polymeric system confirmed the fact that the increase of broadness of XRD peak is evidence for the increase of amorphous fraction [21-23]. At low salt concentration, the intramolecular interactions between the Li^+ and functional groups in both chitosan and methylcellulose chains reduce the crystallinity of the polymer electrolyte system. The polymer electrolyte incorporated with 40 wt.% $LiBF_4$ is expected to host a reasonably fast ionic conduction due to its more amorphous nature (figure 1-i) compared with other polymer electrolyte compositions. When more than 40 wt.% lithium salt was added to the system, some sharp crystalline peaks have appeared at 2θ=13.6°, 21.2°, 23.6°, 31.9°, 32.8°, 36.3°, 40.0°, 48.1°, 50.2°, 53.7°,56.1° and 58.8°. These multiple peaks were attributed to the recrystallization of the $LiBF_4$ salt out of the film surface due to recombination of ions at higher salt concentration.
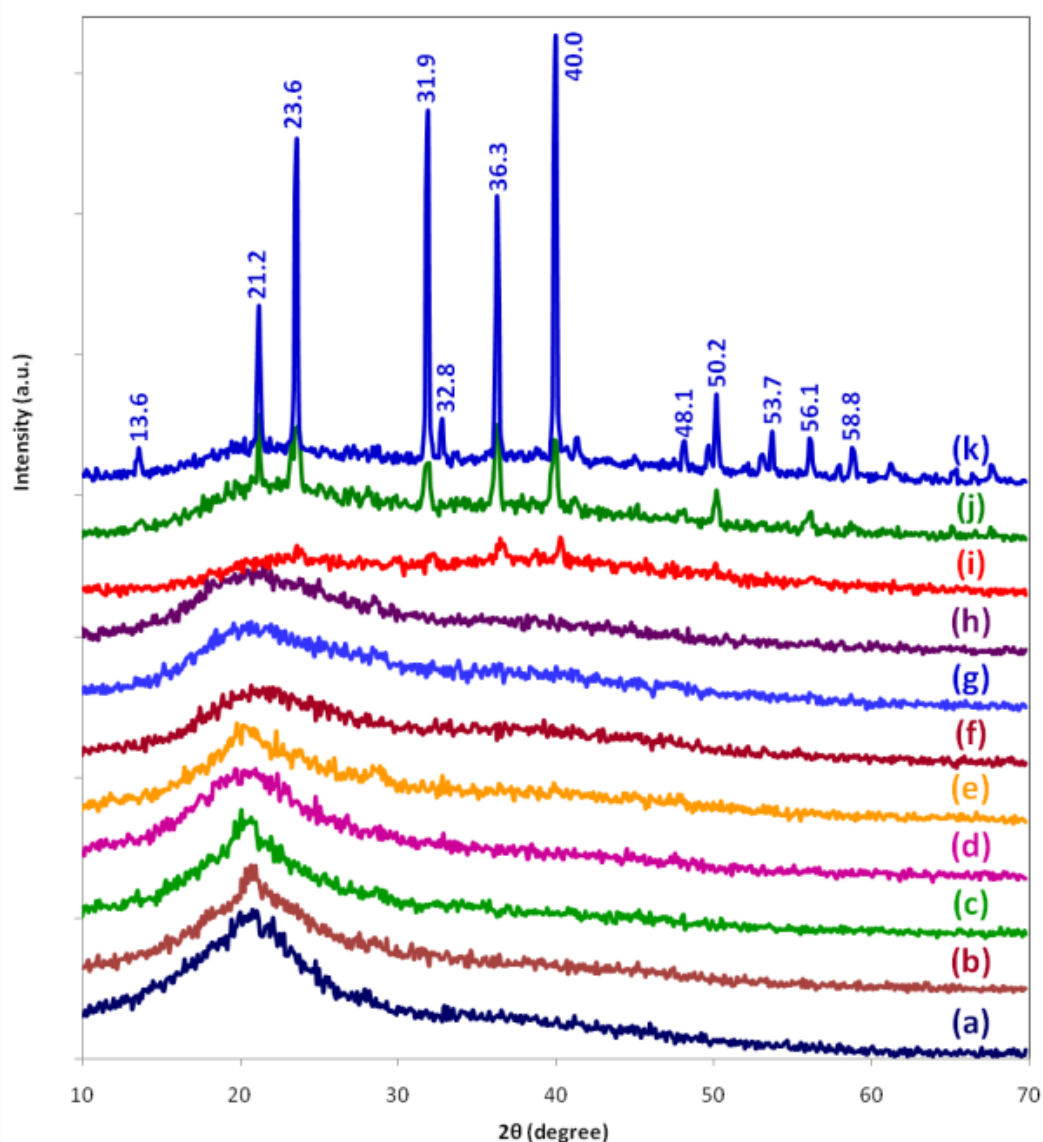
Figure 1. XRD patterns for chitosan-methylcellulose blend film incorporated with (a) 0 wt.% $LiBF_4$, (b) 5 wt.% $LiBF_4$, (c) 10 wt.% $LiBF_4$, (d) 15 wt.% $LiBF_4$, (e) 20 wt.% $LiBF_4$, (f) 25 wt.% $LiBF_4$, (g) 30 wt.% $LiBF_4$, (h) 35 wt.% $LiBF_4$, (i) 40 wt.% $LiBF_4$, (j) 45 wt.% $LiBF_4$ and (k) 50 wt.% $LiBF_4$.

3.2. FTIR analysis

Fourier transform infrared (FTIR) spectroscopy was used to examining the possible interactions between $LiBF_4$ salt and chitosan-methylcellulose polymer blend chains. The infrared spectrum of pure and $LiBF_4$ incorporated chitosan-methylcellulose films are presented in figure 2. From figure 2-a, the hydroxyl band in the spectrum of blend polymer film appear at 3436 cm^{-1}. When $LiBF_4$ salt was added to polymer blend system, this characteristic peak was shifted to lower wavenumbers, reflecting the physical interactions between polymer blend and ions of the salt [24-26].

The carboxamide (O=C–NHR) and the amine (NH_2) bands in the spectrum of the blend film is located at 1645 cm^{-1} and 1561 cm^{-1}, respectively, as shown in figure 3-a. These band positions are almost the same as those reported in other studies [27,28]. For polymer electrolyte samples the position of the carboxamide band has slightly shifted to 1647 cm^{-1}, whereas the amine band was disappeared as shown in figure 3(b-f). This suggests the interactions had taken place between the hydroxyl groups of methylcellulose and Li^+, and between the amino groups of chitosan and BF_4^-. From these FTIR results, it can be concluded that complexation has taken place between $LiBF_4$ salt and the chitosan-methylcellulose blend.
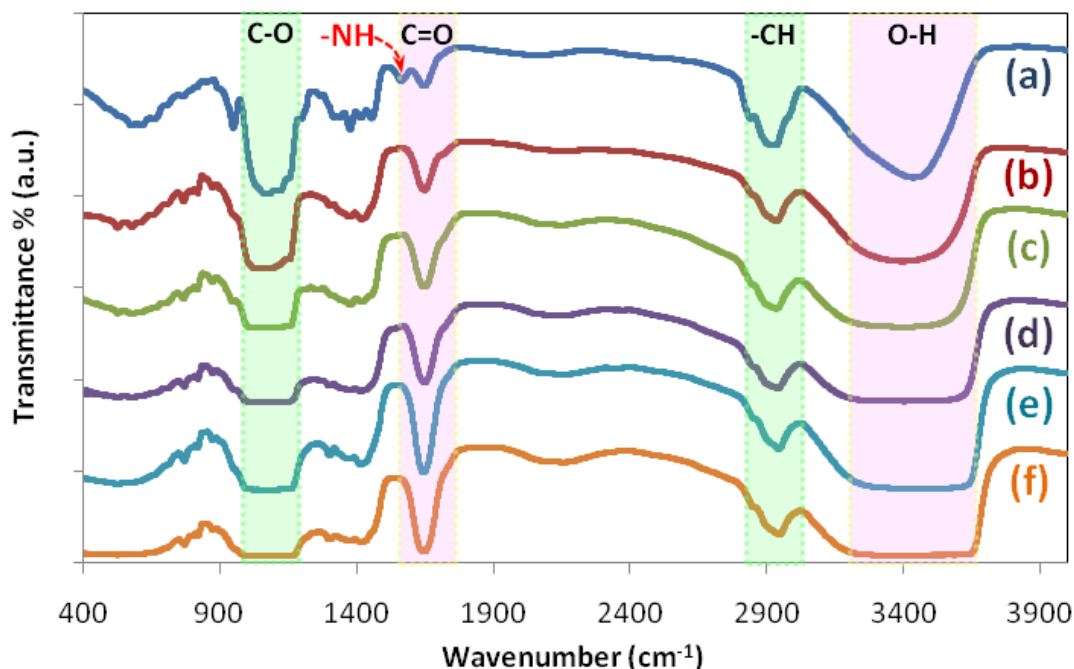
Figure 2. FTIR spectra for chitosan-methylcellulose blend film incorporated with (a) 0 wt.% $LiBF_4$, (b) 10 wt.% $LiBF_4$, (c) 20 wt.% $LiBF_4$, (d) 30 wt.% $LiBF_4$, (e) 40 wt.% $LiBF_4$, (f) 50 wt.% $LiBF_4$.

3.3. SEM study

The SEM micrographs of the solid polymer electrolyte with high salt concentrations are shown in figure 3. It can be noted in figure 3(a, b) that the micrograph of 35 and 40 wt.% $LiBF_4$ film exhibited almost smooth and homogeneous surface, with good structural integrity, indicating that the

lithium salt and polymer blend are miscible in each other. The morphology of the solid polymer electrolytes containing more than 40 wt.% lithium salt reveals the appearance of some solid structures that have suspended out of the surface of the film, as depicted in figure 3(c, d). The XRD analysis revealed that these solid structures are attributed to the recrystallization process of the $LiBF_4$ salt. The inability of the salt to be accommodated by the polymer host resulted in recombination of the ions and recrystallization of the salt [4,29]. This phenomenon reduces the number of mobile ions, which lead to decrease in electrical conductivity as will see later. The same observation was also seen by Kadir et al. [30] for chitosan-PVA-NH_4NO_3 solid polymer electrolyte films.
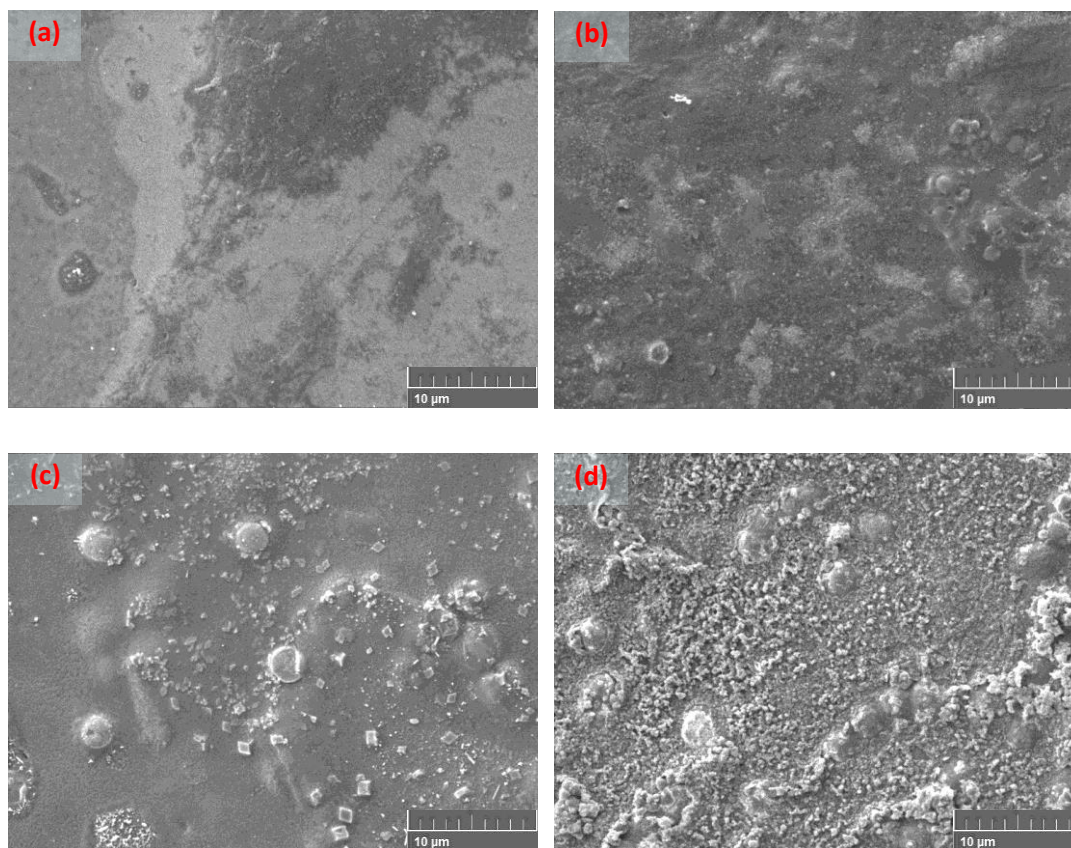
Figure 3. SEM micrographs of chitosan-methylcellulose blend film incorporated with (a) 35 wt.% $LiBF_4$, (b) 40 wt.% $LiBF_4$, (c) 45 wt.% $LiBF_4$, (d) 50 wt.% $LiBF_4$,

3.4. Conductivity study

The ionic conductivity of solid polymer electrolytes depends on the number of charge carriers and their mobility [31]. Hence, when ion concentration is altered by incorporating salt in a polymer matrix, the conductivity is also expected to change [32,33]. Figure 4 represents the frequency-dependence of ac conductivity at different temperatures for chitosan-methylcellulose blend film incorporated with 20 and 40 wt.% $LiBF_4$. The low values of electrical conductivity at low-frequency range is due to the production of a considerable buildup of charge carriers at the electrodes which reduces the effective applied field and hence the conductivity. At higher frequencies, the period of the applied field is too short for the charge to accumulate, thus the conductivity increase [34].

Also, it can be seen clearly, that the values of the conductivity enhanced with increasing $LiBF_4$ salt concentration. This is in agreement with the fact that the amount of Li^+ ions in the blend polymer electrolyte increases with increasing in $LiBF_4$ content.
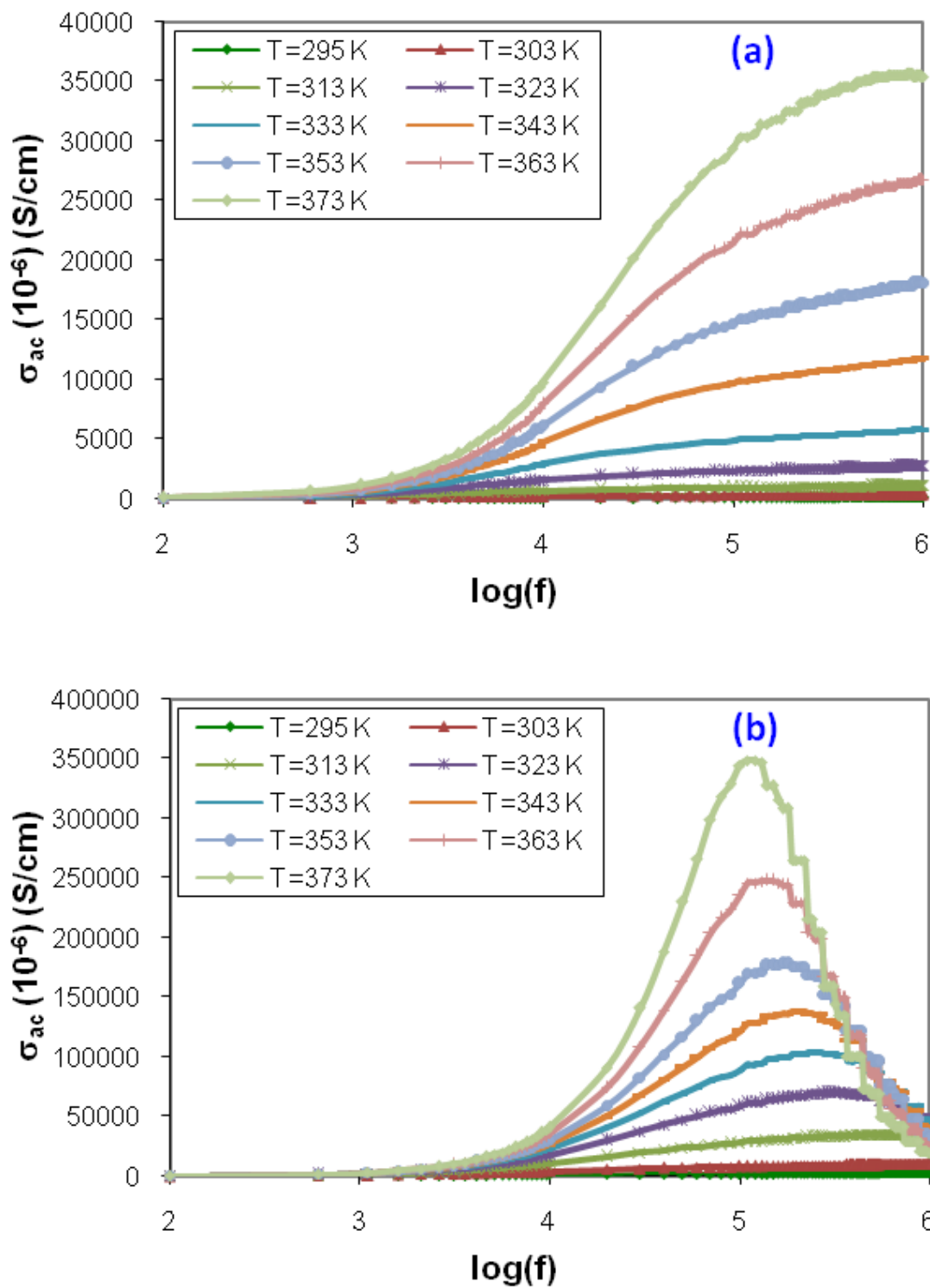
Figure 4. Conductivity versus frequency at various temperature for chitosan-methylcellulose blend film incorporated with (a) 20 wt.% $LiBF_4$, and (b) 40 wt.% $LiBF_4$.

The increase in conductivity with increasing temperature can be ascribed to the increase in both number and mobility of charge carriers in polymer electrolytes [35]. As temperature increases, the polymer chain acquires faster internal modes in which facilitate interchain and intrachain ion hopping movements and, causing, the increase in the conductivity of the polymer electrolyte films [36].

Figure 5 depicts the variation of electrical conductivity versus LiBF$_4$ content at room temperature. It can be seen that the electrical conductivity increases to reach 3.74×10^{-6} S cm^{-1} as the salt concentration increases to 40 wt.%, which mainly related to the increase in the number of lithium-ions [37]. It is interesting to note that the further addition of LiBF$_4$ causes a decrease in the electrical conductivity. For samples contains a large amount of lithium salt (above 40 wt.%), the distance between dissociated ions may become too close that they can recombine to form the salt which does not contribute to electrical conductivity [30]. This result was supported by the XRD and SEM analysis that clearly showed the formation of the LiBF$_4$ salt crystals on the surface of the polymer electrolyte samples at high salt concentrations.
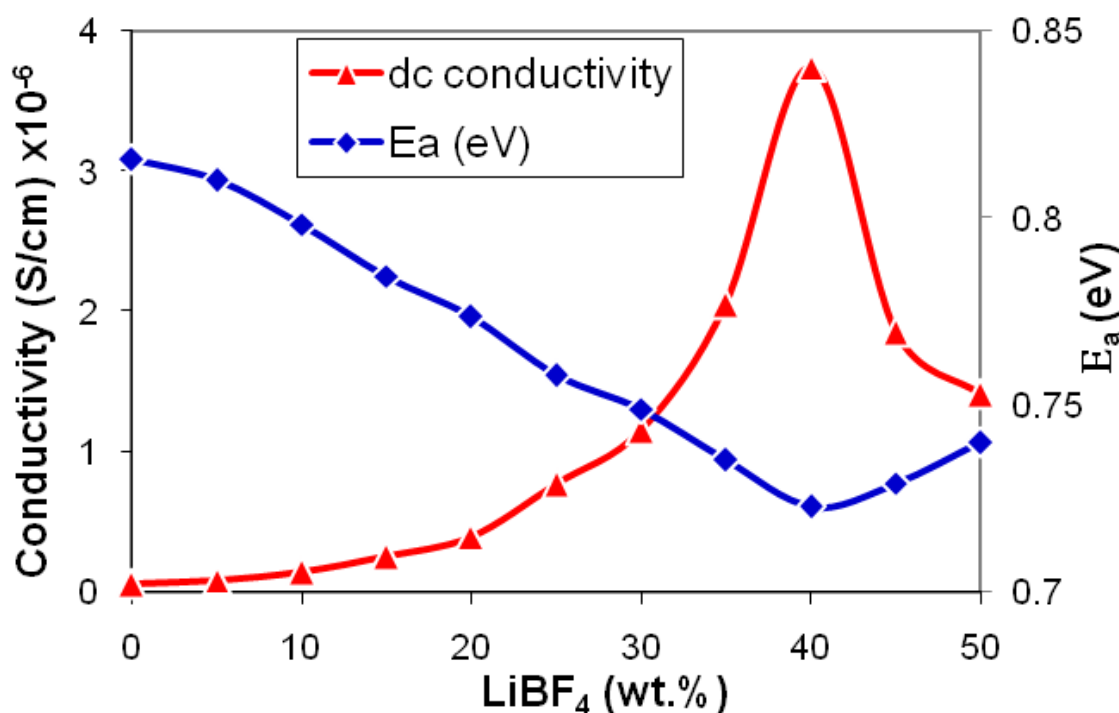
Figure 5. Effect of LiBF$_4$ content on the conductivity and the activation energy of polymer electrolyte at room temperature.

The linear variation of dc conductivity versus temperature shown in figure 6 suggests an Arrhenius-type thermal activated process for the present solid polymer blend electrolyte; hence, the conductivity can be expressed as:

$$\sigma = \sigma_o \exp\left(\frac{-E_a}{k_B T}\right) \qquad (1)$$

where σ_o is a pre-exponential factor, E_a is the activation energy of electrical conduction, k_B is the Boltzmann constant and T is the temperature in Kelvin.

The activation energy E_a, which is a combination of the energy of defect formation and the energy of defect migration, is calculated from the slope of the straight lines in figure 6. The variation of E_a versus LiBF$_4$ concentration is presented in figure 5. It can be seen that the activation energy decreases with increasing conductivity. The highest conducting sample has the lowest activation energy of 0.72 eV. This result denotes that the lithium ions in highly conducting samples require lower energy for migration. Moreover, the low activation energy can result from the short distance between transit sites provided by the blended biopolymers [27].
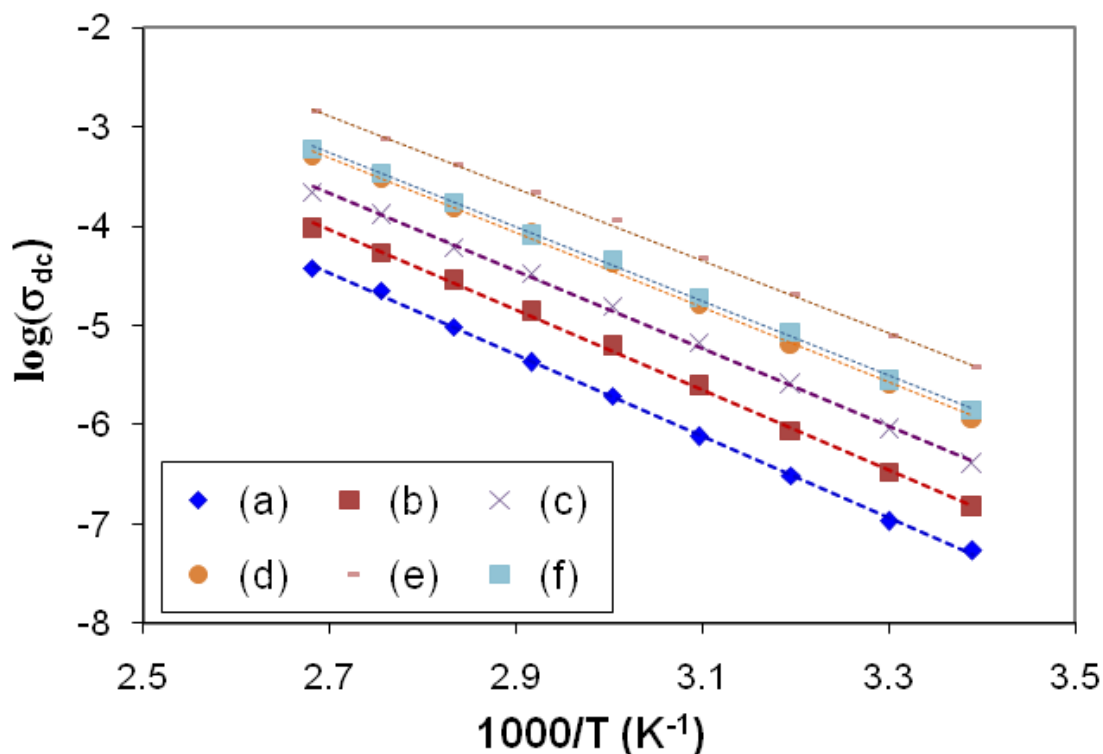
Figure 6. Temperature dependence dc conductivity for chitosan-methylcellulose blend film incorporated with (a) 0 wt.% LiBF$_4$, (b) 10 wt.% LiBF$_4$, (c) 20 wt.% LiBF$_4$, (d) 30 wt.% LiBF$_4$, (e) 40 wt.% LiBF$_4$, (f) 50 wt.% LiBF$_4$.

3.5. Dielectric analysis

Dielectric study of the polymeric materials provides essential insights into the polarization effect at the electrode/electrolyte interface and help to promote understanding the conductivity behavior of polymer electrolyte [38]. The dielectric constant ε' for the prepared polymer electrolyte films were calculated over a wide range of frequency between 100 Hz and 1MHz, and at a temperature range of 295 K to 373 K, using [39]:

$$\varepsilon' = \frac{C_p \, d}{\varepsilon_o \, A} \qquad (2)$$

where C_p is capacitance value measured using LCR meter, and ε_o is permittivity of free space. The frequency dependence of ε' is shown in figures 7. It can be seen that the value of ε' increase as the frequency decreases. At low frequencies, ε' rise due to the electrode polarization and space charge

effects [37]. However, at high frequencies, the periodic reversal of the applied electric field occurs quickly, hence, no excess ions accumulation in the electrical field direction [40], thus the observed decrease in the value of ε' occurs as a result of a decrease in the polarization.
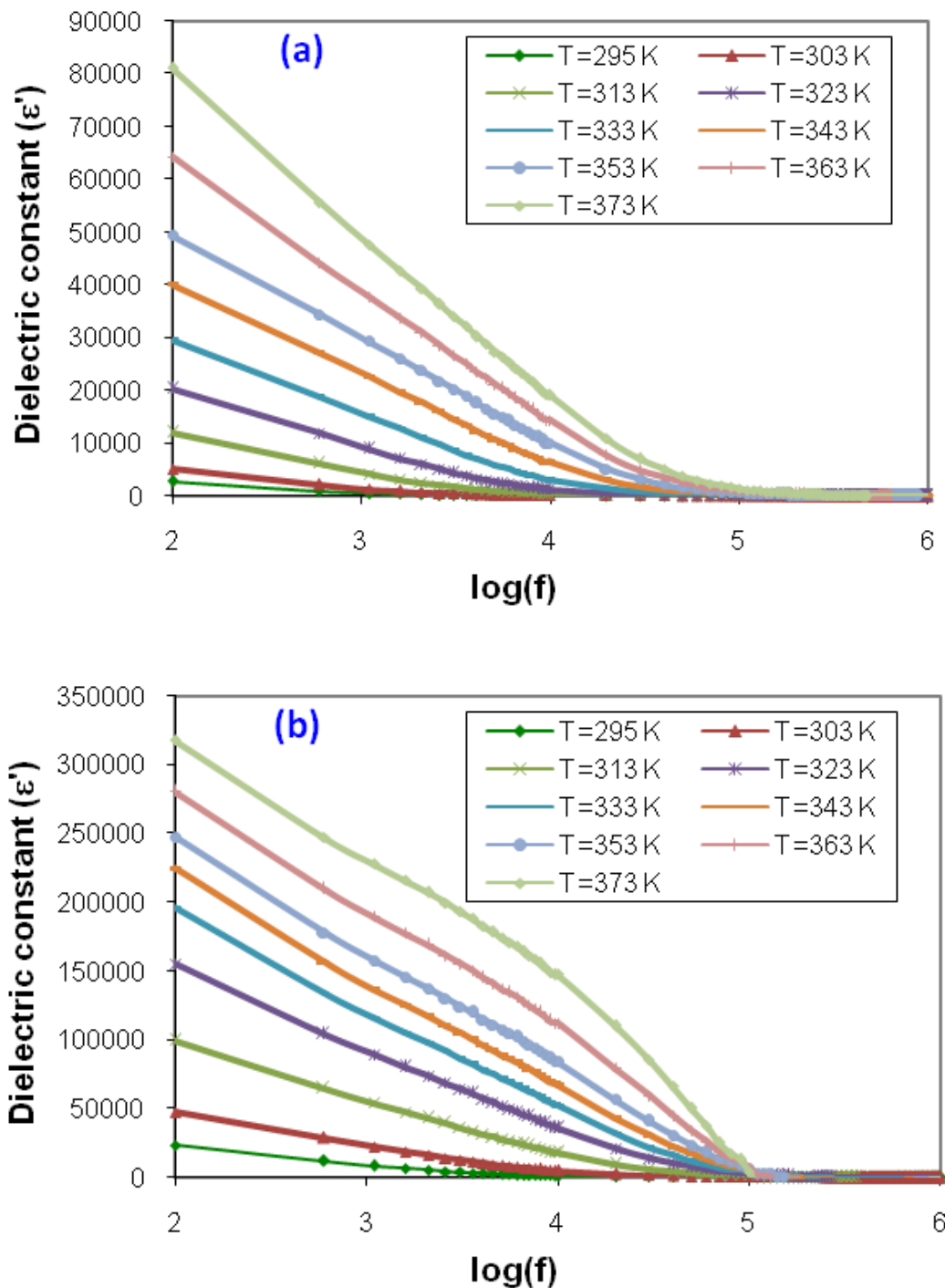
Figure 7. Dielectric constant versus frequency at different temperatures for chitosan-methylcellulose blend film incorporated with (a) 20 wt.% LiBF$_4$, and (b) 40 wt.% LiBF$_4$.

Moreover, the decrease in ε' with increasing frequency can be associated to the inability of dipoles to follow the applied field in order to rotate rapidly, leading to a lag between the frequency of oscillating dipole and that of the electrical field [1]. It is well established in the literature that the sharp increase of the low frequencies ε', is due to the impact of electrode/electrolyte interface [41,42].

By comparison results in figures 4 and 7, it is observed that the highest electrical conducting sample has the highest value of ε'. Such high dielectric constant ε' values demonstrate that the high ionic conductivity mainly due to the enhanced charge carrier density at the space charge accumulation region due to electrode/electrolyte interface. The variation of dielectric constant ε' for PVA-chitosan-NH_4Br system reported by Yusof et al. [43] also follows the same trend as their conductivity result.

3.6. Transport parameters

Rice and Roth [44] proposed an attractive model for fast ionic conductors, based on the hypothesis that in an ionic conductor, the conducting ions of mass m belonging to the conducting spaces can be thermally excited from localized ionic states to free ion-like states, and the ion propagates throughout the spaces with a velocity v and energy $E = \frac{1}{2}mv^2$. Recently this model was extensively used to provide an estimation of the number density of mobile ions that assist the electrical conduction in the polymer electrolyte systems [45]. According to this model, electrical conductivity can be expressed as:

$$\sigma = \frac{2}{3}\left[\frac{(Ze)^2}{mk_BT}\right]nE_a\tau\exp\left(\frac{-E_a}{k_BT}\right) \qquad (3)$$

where Z is the valency of conducting species, e is the electron charge, m is the mass of the ions, n is the number density of ions, E_a is the activation energy, and τ is the traveling time of the ions which can be calculated using the equation:

$$\tau = \frac{l}{v} \qquad (4)$$

where l is a distance between two coordinating sites across which the ions may hop. According to Shukur et al. [46], l can be considered as the jump distance between two complexation sites and taken to be around 10.4 Å, which is used in this study. From the number density of ions (n) calculated from equation 3, the ionic mobility μ can be calculated using this equation [34]:

$$\mu = \frac{\sigma}{ne} \qquad (5)$$

The calculated transport parameters as a function of lithium salt concentration are listed in Table 1. The n values are in the range 5.84×10^{23} to 8.37×10^{23} cm^{-3}, and μ values lies between 9.58×10^{-15} and 2.80×10^{-13} cm^2 V^{-1} s^{-1}. In general, the electrical conductivity is dependent on the mobile ion concentration and their mobility ($\sigma = en\mu$) [47]. It can be seen from Table 1 that the increasing conductivity value with increasing lithium salt is influenced by the increasing number density and mobility of Li^+ ions. The highest conducting sample with the addition of 40 wt% $LiBF_4$ has the highest n and μ values of 8.37×10^{23} cm^{-3} and 2.80×10^{-13} cm^2 V^{-1} s^{-1}, respectively. As more salt added, the values of n and μ decreases, leading to a drop in electrical conductivity.

Table 1. The transport parameters of the chitosan-methylcellulose-LiBF$_4$ blend electrolyte films at room temperature.

LiBF$_4$ wt.%	σ (S cm^{-1})	E_a (eV)	v (m/s)	τ (s)	n (cm^{-3})	μ (cm^{2}V^{-1}s^{-1})
5	8.96×10^{-8}	0.810	4729.47	2.20×10^{-13}	5.84×10^{23}	9.58×10^{-15}
10	1.46×10^{-7}	0.798	4695.17	2.22×10^{-13}	6.05×10^{23}	1.51×10^{-14}
15	2.55×10^{-7}	0.784	4654.15	2.23×10^{-13}	6.19×10^{23}	2.58×10^{-14}
20	3.95×10^{-7}	0.773	4621.67	2.25×10^{-13}	6.28×10^{23}	3.93×10^{-14}
25	7.71×10^{-7}	0.757	4574.61	2.27×10^{-13}	6.69×10^{23}	7.20×10^{-14}
30	1.15×10^{-6}	0.749	4547.59	2.29×10^{-13}	7.09×10^{23}	1.02×10^{-13}
35	2.06×10^{-6}	0.735	4505.83	2.31×10^{-13}	7.44×10^{23}	1.73×10^{-13}
40	3.75×10^{-6}	0.722	4467.37	2.33×10^{-13}	8.37×10^{23}	2.80×10^{-13}
45	1.85×10^{-6}	0.729	4486.95	2.32×10^{-13}	5.29×10^{23}	2.19×10^{-13}
50	1.41×10^{-6}	0.740	4520.40	2.30×10^{-13}	6.15×10^{23}	1.44×10^{-13}

3.7. Conduction mechanism

In general, at a constant temperature, the frequency-dependence ac conductivity (σ_{ac}) is analyzed at a high-frequency region to comprehend the ion conduction mechanism using Jonscher power law [48,49]:

$$\sigma(\omega) = \sigma(0) + A\omega^s, \qquad 0 < s < 1 \qquad (6)$$

where $\sigma(\omega)$ is the total conductivity, $\sigma(0)$ is frequency-independent dc conductivity, A is a pre-factor that depends on composition and temperature, and s is an exponent of the power law. The value of exponent s is obtained from the slopes of the plots of $\log(\sigma_{ac})$ versus $\log(\omega)$ in the frequency range $4.75 \leq \log(\omega) \leq 5.75$, as shown in figure 8. Numerous reports suggest that the acceptable frequency range to find frequency exponent (s) is in the high-frequency region [50,51].
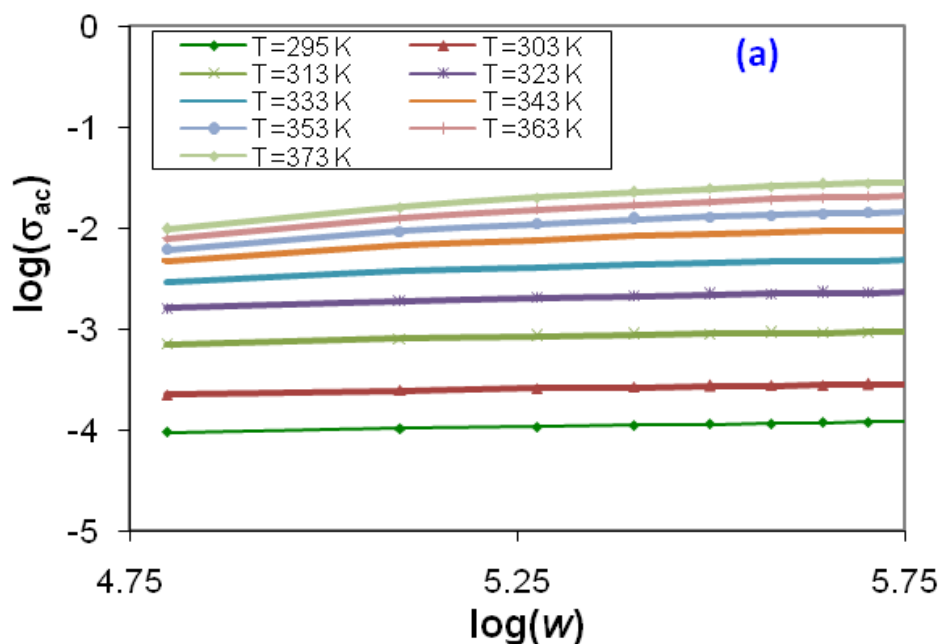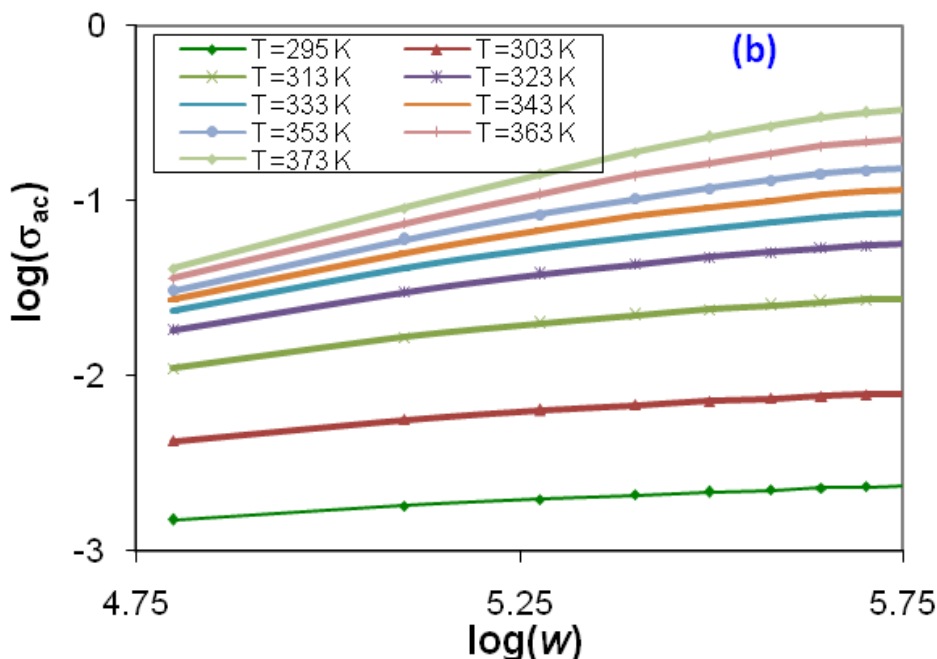
Figure 8. Variation of $\log(\sigma_{ac})$ versus $\log(\omega)$ at different temperatures for chitosan-methylcellulose blend film incorporated with (a) 20 wt.% LiBF$_4$, and (b) 40 wt.% LiBF$_4$.

Table 2. The value of s versus T for chitosan-methylcellulose-LiBF$_4$ solid polymer electrolyte system.

Temperature (K)	Frequency exponent (s)									
	5 wt.%	10 wt.%	15 wt.%	20 wt.%	25 wt.%	30 wt.%	35 wt.%	40 wt.%	45 wt.%	50 wt.%
295	0.823	0.789	0.530	0.164	0.445	0.216	0.138	0.174	0.205	0.179
303	0.816	0.744	0.449	0.123	0.465	0.282	0.107	0.232	0.168	0.095
313	0.787	0.661	0.300	0.087	0.485	0.380	0.126	0.344	0.06	0.087
323	0.737	0.550	0.198	0.086	0.534	0.458	0.180	0.424	0.072	0.109
333	0.697	0.444	0.124	0.098	0.588	0.519	0.234	0.485	0.131	0.164
343	0.573	0.304	0.088	0.121	0.649	0.592	0.296	0.543	0.225	0.261
353	0.458	0.205	0.072	0.140	0.709	0.665	0.355	0.600	0.303	0.379
363	0.358	0.145	0.062	0.156	0.773	0.720	0.425	0.668	0.370	0.497
373	0.293	0.118	0.053	0.158	0.812	0.780	0.498	0.723	0.443	0.457

The variations of s against temperature for chitosan-methylcellulose-LiBF$_4$ solid polymer electrolyte system at different salt concentration are presented in Table 2. It can clearly be seen that the variation of exponent s versus temperature altered by change in LiBF$_4$ concentration. The decreasing trend of exponent s with increasing temperature for 5, 10, 15 wt.% LiBF$_4$ suggests that the conduction mechanism can be represented by the correlated barrier hopping (CBH) model. However for 20 wt.% LiBF$_4$ the value of s is observed to be almost temperature-independent. Thus the quantum mechanical tunneling (QMT) is the most appropriate model to describe the conduction mechanism of this composition. The increasing trend of exponent s with increasing temperature for high salt

concentration (25, 30, 35, 40, 45, 50 wt.% LiBF$_4$) indicates that the non-overlapping small polaron tunneling (NSPT) model is most suitable for these compositions.

4. CONCLUSION

Chitosan-methylcellulose blend polymer electrolyte films incorporated with various LiBF$_4$ content were successfully prepared by a solution casting method. From the XRD results, 40 wt.% LiBF$_4$ was found to be the most amorphous composition. From FTIR studies, the complexation between lithium salt and polymer blend was confirmed by the shift of hydroxyl, amine and carboxamide bands of the chitosan-methylcellulose blend film. The highest room temperature electrical conductivity of 3.74×10^{-6} S cm^{-1} was achieved at 40 wt.% LiBF$_4$. SEM studies further verified this result. Dielectric studies suggest that the solid polymer electrolyte systems in this study have non-Debye behavior. The conductivity-temperature dependence of the present electrolyte films obeyed the Arrhenius rule. Employing the Rice and Roth model, the highest conducting sample has the highest n and μ values of 8.37×10^{23} cm^{-3} and 2.80×10^{-13} cm^2 V^{-1} s^{-1}, respectively. Thus, the ionic conductivity variation is mainly due to the concentration and mobility of lithium ions. The conduction mechanism was found to be correlated barrier hopping (CBH) model at low salt concentration and change to the non-overlapping small polaron tunneling (NSPT) model at higher salt concentration.

References

1. K. Ramly, M.I.N. Isa, and A.S.A. Khiar, *Mater. Res. Innov.*, 15 (2011) S82.
2. L.S. Ng, and A.A. Mohamad, *J. Power Sources*, 163 (2006) 382.
3. I. Riess, *Solid State Ionics*, 136-137 (2000) 1119.
4. S.B. Aziz, O.G. Abdullah, M.A. Rasheed, and H.M. Ahmed, *Polymers*, 9 (2017) 187.
5. N.A.N. Aziz, N.K. Idris, and M.I.N. Isa, *Int. J. Polym. Anal. Charact.*, 15 (2010) 319.
6. S.B. Aziz, O.G. Abdullah, and M.A. Rasheed, *J. Appl. Polym. Sci.*, 134 (2017) 44847.
7. O.G. Abdullah, S.B. Aziz, and M.A. Rasheed, *Ionics*, DOI: 10.1007/s11581-017-2228-1 (2017).
8. D.S. Vicentini, A.J. Smania, and M.C.M. Laranjeira, *Mater. Sci. Eng. C*, 30 (2010) 503.
9. S.B. Aziz, O.G. Abdullah, D.R. Saber, M.A. Rasheed, and H.M. Ahmed, *Int. J. Electrochem. Sci.*, 12 (2017) 363.
10. A.S.A. Khiar, R. Puteh, and A.K. Arof, *Physica B*, 373 (2006) 23.
11. N.E.A. Shuhaimi, L.P. Teo, H.J. Woo, S.R. Majid, and A.K. Arof, *Polym. Bull.*, 69 (2012) 807.
12. Y.N. Sudhakar, and M. Selvakumar, *Electrochim. Acta*, 78 (2012) 398.
13. S. Ibrahim, M.M. Yassin, R. Ahmad, and M.R. Johan, *Ionics*, 17 (2011) 399.
14. I.S.M. Noor, S.R. Majid, A.K. Arof, D. Djurado, S.C. Neto, and A. Pawlicka, *Solid State Ionics*, 225 (2012) 649.
15. M.F. Shukur, R. Ithnin, and M.F.Z. Kadir, *Ionics*, 22 (2016) 1113.
16. M. Ulaganathan, and S. Rajendran, *J. Appl. Polym. Sci.*, 118 (2010) 646.
17. N.L.M. Zazuli, and A.S.A. Khiar, *Appl. Mech. Mater.*, 719-720 (2015) 82.

18. O.G. Abdullah, R.R. Hanna, and Y.A.K. Salman, *J. Mater. Sci. Mater. Electron.*, 28 (2017) 10283.
19. M. Hasegawa, A. Isogai, F. Onabe, M. Usuda, and R.H. Atalla, *J. Appl. Polym. Sci.*, 45 (1992) 1873.
20. O.G. Abdullah, Y.A.K. Salman, and S.A. Saleem, *Phys. Mater. Chem.*, 3 (2015) 18.
21. S.B. Aziz, M.A. Rasheed, S.R. Saeed, and O.G. Abdullah, *Int. J. Electrochem. Sci.*, 12 (2017) 3263.
22. O.G. Abdullah, *J. Mater. Sci. Mater. Electron.*, 27 (2016) 12106.
23. S.F. Bdewi, O.G. Abdullah, B.K. Aziz, and A.A.R. Mutar, *J. Inorg. Organomet. Polym. Mater.*, 26 (2016) 326.
24. O.G. Abdullah, S.B. Aziz, D.R. Saber, R.M. Abdullah, R.R. Hanna, and S.R. Saeed, *J. Mater. Sci. Mater. Electron.*, 28 (2017) 8928.
25. Y.J. Yin, K.D. Yao, G.X. Cheng, and J.B. Ma, *Polym. Int.*, 48 (1999) 429.
26. O.G. Abdullah, Y.A.K. Salman, and S.A. Saleem, *J. Mater. Sci. Mater. Electron.*, 27 (2016) 3591.
27. M.H. Buraidah, and A.K. Arof, *J. Non-Cryst. Solids*, 357 (2011) 3261.
28. M.F.Z. Kadir, Z. Aspanut, S.R. Majid, and A.K. Arof, *Spectrochim. Acta A*, 78 (2011) 1068.
29. M.F. Shukur, and M.F.Z. Kadir, *Electrochim. Acta*, 158 (2015) 152.
30. M.F.Z. Kadir, S.R. Majid, and A.K. Arof, *Electrochim. Acta*, 55 (2010) 1475.
31. S.B. Aziz, O.G. Abdullah, and M.A. Rasheed, *J. Mater. Sci. Mater. Electron.*, 28 (2017) 12873.
32. O.G. Abdullah, S.B. Aziz, and M.A. Rasheed, *Results in Physics*, 6 (2016) 1103.
33. M. Kumar, T. Tiwari, and N. Srivastava, *Carbohydr. Polym.*, 88 (2012) 54.
34. C.S. Ramya, S. Selvasekarapandian, T. Savitha, G. Hirankumar, R. Baskaran, M.S. Bhuvaneswari and P.C. Angelo, *Eur. Polym. J.*, 42 (2006) 2672.
35. S.B. Aziz, O.G. Abdullah, S.A. Hussein, and H.M. Ahmed, Polymers, 9 (2017) 622.
36. R. Baskaran, S. Selvasekarapandian, G. Hirankumar, and M.S. Bhuvaneswari, *Ionics*, 10 (2004) 129.
37. A.S.A. Khiar, and A.K. Arof, *Ionics*, 16 (2010) 123.
38. Y.M. Yusof, M.F. Shukur, H.A. Illias, and M.F.Z. Kadir, *Phys. Scr.*, 89 (2014) 035701.
39. O.G. Abdullah, and S.A. Saleem, *J. Electron. Mater.*, 45 (2016) 5910.
40. S. Ramesh, and A.K. Arof, *Mater. Sci. Eng. B*, 85 (2001) 11.
41. M.L. Verma, and H.D. Sahu, *Ionics*, 21 (2015) 3223.
42. M. Ravi, Y. Pavani, K.K. Kumar, S. Bhavani, A.K. Sharma, and V.V.R.N. Rao, *Mater. Chem. Phys.*, 130 (2011) 442.
43. Y.M. Yusof, H.A. Illias, and M.F.Z. Kadir, *Ionics*, 20 (2014) 1235.
44. M.J. Rice, and W.L. Roth, *J. Solid State Chem.*, 4 (1972) 294.
45. N.E.A. Shuhaimi, L.P. Teo, S.R. Majid, and A.K. Arof, *Synt. Met.*, 160 (2010) 1040.
46. M.F. Shukur, R. Ithnin, H.A. Illias, and M.F.Z. Kadir, *Opt. Mater.*, 35 (2013) 1834.
47. S.R. Majid, and A.K. Arof, *Physica B*, 355 (2005) 78.
48. R. Murugaraj, G. Govindaraj, and D. George, *Mater. Lett.*, 57 (2003) 1656.
49. G.C. Psarras, E. Manolakaki, and G.M. Tsangaris, *Composites A*, 34 (2003) 1187.
50. M.H. Buraidah, L.P. Teo, S.R. Majid, and A.K. Arof, *Physica B*, 404 (2009) 1373.
51. M.F.Z.A. Kadir, L.P. Teo, S.R. Majid, and A.K. Arof, *Mater. Res. Innov.*, 13 (2009) 259.